Amplification effect of cascading breach discharge of landslide dams

Amplification effect of cascading breach discharge of landslide dams

Hongchao Zheng[1], Zhenming Shi[1], Ming Peng[1]*, Shenggong Guan[2]*, Kevin J Hanley[3], Shijin Feng[1]

[1]Key Laboratory of Geotechnical and Underground Engineering of the Ministry of Education, and Department of Geotechnical Engineering, College of Civil Engineering, Tongji University, China

[2]Key Laboratory of Rock Mechanics and Geohazards of Zhejiang Province, Shaoxing University, China

[3]School of Engineering, Institute for Infrastructure and Environment, The University of Edinburgh, United Kingdom

*corresponding author: Ming Peng, E–mail: pengming@tongji.edu.cn

Shenggong Guan, E–mail: guanshg@163.com

Abstract Affected by earthquakes and heavy rainfall, multiple landslide dams often cluster closely together along river reaches or gullies. Compared with a single landslide dam, the burst flood produced by the cascading failure of multiple landslide dams can be enhanced, seriously threatening life and property downstream. Here, we conduct a series of experiments in a 42 m flume to investigate the failure mechanisms of single and paired dams with fine-grained, well graded and coarse-grained debris, analyze the effects of dam geometry and initial water level of a downstream dam on the cascading breach, and quantitatively evaluate the amplification effect of cascading breach discharge. Single dams fail by overtopping along with seepage instability for a fine-grained dam, headcutting for a well graded dam and overtopping for a coarse-grained dam, respectively. The type of failure which occurs for a single dam is influenced by the shear strength of the dam material and seepage. However, the downstream dams in cascading tests fail by overtopping irrespective of dam material due to the large outburst floods from the upstream dams. A general flat slope angle is maintained during breaching for the fine-grained and coarse-grained dams, while a step-pool structure is developed for the well graded dams because the finer grains are easier to wash away than coarse grains. The peak breach discharge for a downstream dam is 1.4–1.9 times the value for an upstream dam in the experimental runs, indicating the amplification effect of breach discharge. The amplification effect has a negative linear correlation with the time interval between the peak breach discharges of the two dams because the overlap of breach processes of upstream and downstream dams is gradually reduced as the time interval increases.

Keywords: Landslide dams, cascading failure, failure type, breach discharge, amplification effect

1. Introduction

Landslide dams are natural dams formed by river blockages with plenty of debris materials from landslides, avalanches, or debris flows (Costa and Shuster, 1988, Clague and Evans, 1994; Fan et al., 2012; Peng and Zhang, 2012; Shi et al., 2018; Shan et al., 2020; Gong et al., 2021). Landslide dams have frequently been triggered by earthquakes, extreme climate hazards and snowmelt (Korup, 2004; Korup, 2005; Takahashi, 2007; Strom, 2010; Dong et al., 2011; Shen et al., 2020). Multiple landslide dams are often closely distributed along river reaches or gullies: for instance, dozens of landslide dams clustered along river reaches induced by the 1999 Chi-Chi earthquake (Liao and Lee, 2000), the 2004 Chuetsu earthquake (Wang et al., 2007) and the 2008 Wenchuan earthquake (Fan et al., 2012). As many as eighteen landslide dams were formed by the 2009 Morakot typhoon in Taiwan (Chen and Chang, 2016). At least nineteen landslide dams in the Sanyanyu gully were destroyed by upland flash floods and developed into a catastrophic debris flow in Zhouqu (Cui et al., 2013).

Landslide dams present serious threats to life and property downstream from a potentially rapid release of the impounded water (Hancox et al., 2005; Davies et al., 2007; Huang and Fan, 2013; Zheng et al., 2018). The outburst flood released by an upstream landslide dam can induce failures of downstream landslide dams one after another (Shi et al., 2015). Compared with a single landslide dam, the cascading failure

of multiple landslide dams is more complicated (Zhou et al., 2013). The cascading breach of landslide dams may result in a sharp increase in the peak outflow rate and thus a more serious disaster downstream. The hazard mitigation measure appropriate for a single landslide dam may not be adequate for multiple landslide dams. Therefore, a clear understanding of the failure mechanism and cascading outburst flood of multiple landslide dams is crucial before taking any effective mitigation measures.

Many research studies have been conducted to investigate the physical mechanisms that govern the failure of single landslide dams (Coleman et al., 2002; Awal et al., 2008; Schmocker and Hager, 2009; Walder et al., 2015; Jiang et al., 2018; Zhou et al., 2019; Peng et al., 2021). Both laboratory experiments and field surveys show that dam failure usually originates from overtopping and headcutting which arises at the toe of the dam's downstream face and progressively migrates upstream to the lake (Gregoretti et al., 2010). Landslide dams are usually made of a heterogeneous mass of unconsolidated or poorly consolidated material and thus may be subject to intense seepage flows (Shi et al., 2018). Several seepage erosion processes can also lead to dam failure: internal erosion, piping, and seepage instability (slide of a downstream dam slope). According to Takahashi (2007) and Chen et al. (2015), failure type is regulated by dam permeability and material strength. Overtopping is likely to occur with small permeability and high strength, while sudden slide collapse that is induced by internal instability is possibly associated with higher permeability and weaker strength. The effect of grain composition on the failure type has been explored only for a single landslide dam. Whether these research findings are

applicable to multiple landslide dams is still unknown.

The research attention paid to the cascading failure of landslide dams has been relatively limited. Niu et al. (2012) claimed that the cascading peak discharges of the Xiaogangjian and Yibadao landslide dams were decreased by 20% by reducing the heights of both landslide dams. Nevertheless, it is not clear which mitigation measures should be applied to each of the landslide dams to reduce the peak discharge most effectively. Cao et al. (2011) and Zhou et al. (2013) compared the breach processes of single and multiple landslide dams and found that the magnitudes of the flows increased by 15%–60% after a cascading failure of landslide dams. Shi et al. (2015) analyzed the cascading breach of the Tangjiashan landslide dam and two other downstream dams with a physically-based breach model and observed that multi-peak floods were very likely to develop at the downstream landslide dam. However, the effects of grain composition and geometry of the landslide dams on the cascading failure and the amplification effect of breach discharge have not been explored.

The structure of the paper is as follows. Firstly, the experimental flume setup, grain composition and experimental design are described. Then, we discern the types of failure that occur for single and paired dams and compare the breach processes of dams with different grain compositions. Additionally, the effects of grain composition, dam geometry and initial water level of downstream dams on the cascading failure are investigated. Finally, we discuss the differences between failure types for single and paired dams, the condition for the amplification effect of cascading breach discharge, the reasons for the occurrence of multiple peaks in the discharge hydrographs, and the

geometrical characteristics of the residual dams.

2. Flume tests on landslide dams

Two model dams were constructed in our experiments to reproduce the cascading breach process of landslide dams. According to field surveys, an upstream landslide dam with a larger lake volume can have a significant influence on a downstream landslide dam with a smaller lake volume, such as the Tangjiashan and Kuzuba dams (Shi et al., 2015) as well as the Xiaogangjian and Yibadao dams (Chen et al., 2018). Conversely, an upstream landslide dam with a smaller lake volume has a limited effect on a downstream landslide dam with a larger lake volume, as the latter has sufficient capacity to contain the outburst flood from the upstream dam. Therefore, a model dam with a larger height was located upstream of a model dam with a smaller height.

2.1 Experimental setup

All experiments were conducted in the flume system located at Tongji University (Figs. 1 and 2). The flume system consisted of a reservoir with a volume of 36 m^3 (3 m x 4 m x 3 m), a water flooding pump with a maximum inflow rate of 0.1 m^3/s, a straight flume, and a dewatering pump with a maximum outflow rate of 0.1 m^3/s. The flume had a length of 42 m, a width of 0.80 m and a height of 1.25 m. The bottom, front and rear of the flume were made of reinforced concrete. The flume sidewalls were made of transparent tempered glass, allowing the breach process of landslide dams to be observed. The flume bottom was horizontal, considering that the longitudinal gradient of Tangjiashan landslide dam during breaching was limited to

0.006 (Peng et al., 2014). A cluster of plastic floats was placed close to the point of inflow to eliminate the wave from the water flooding pump. The water at the downstream end of the flume was extracted by the dewatering pump and thus the water level in this region was kept close to zero.

As shown in Fig. 1, two cameras (EOS550D, Canon, 5184 x 3456 pixel) were located at the side of the flume in order to record the water level and the breach processes of the upstream and downstream dams. Two video cameras (GZ-R10BAC, JVC, 1920 x 1080 pixel) with a sample frequency of 25 Hz were suspended above the upstream and downstream dams to record the overflow process of an outburst flood. In addition, another video camera of the same type was fixed in the flume to record the breach process of the downstream dam.

The inflow rate for the upstream dam was held constant and the upstream water level was steadily changed. One camera combined with a steel tape was employed to accurately record the upstream water level and calculate the breach discharge by means of the continuity equation. For the downstream dam, the inflow rate was due to the outburst flood from the upstream dam so the water level may fluctuate. Three more video cameras (GZ-R10BAC, JVC, 1920 x 1080 pixel) in tandem with equally spaced steel tapes were used to record the water level impinging on the downstream dam.

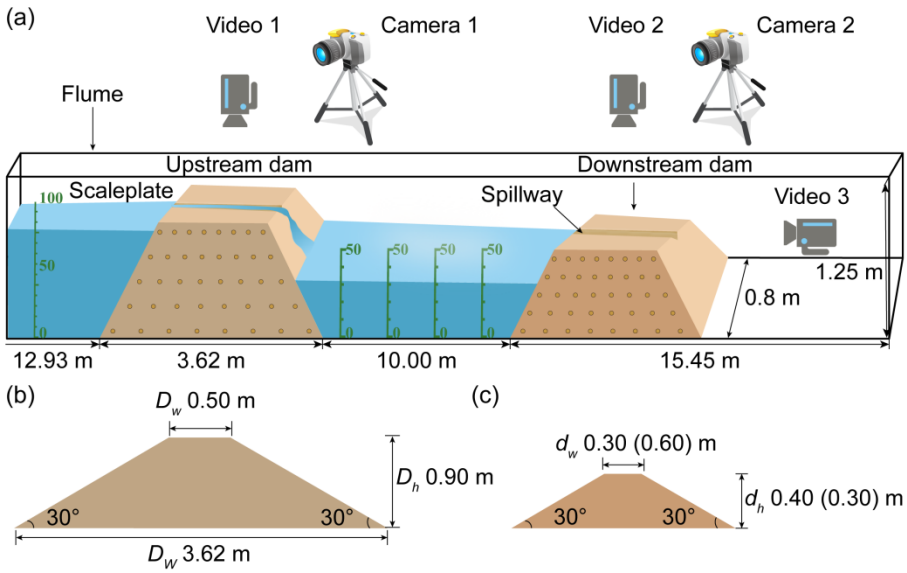

Fig. 1. Schematic diagram of experimental apparatus. (a) Two model dams located in the experimental flume. (b) Longitudinal section of upstream model dam. (c) Longitudinal section of downstream model dam.

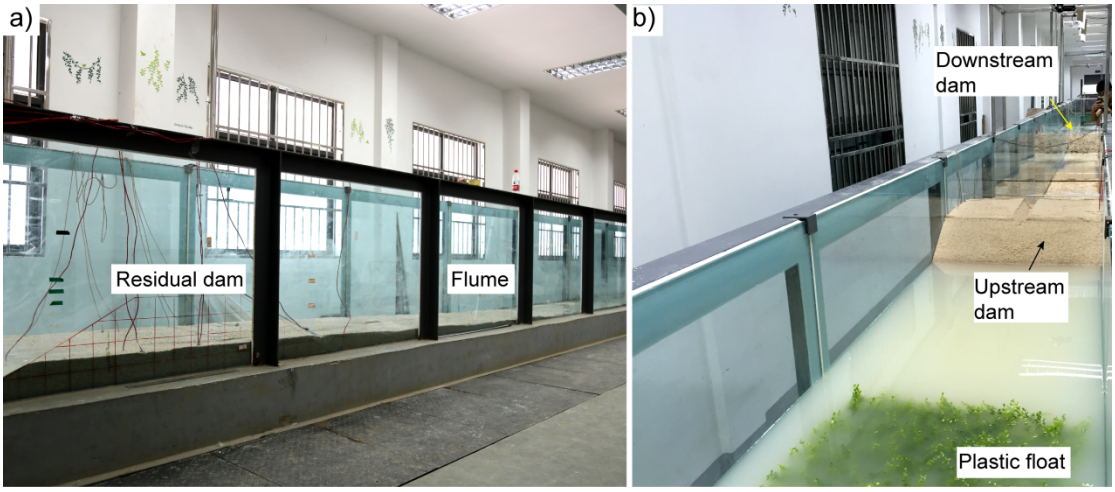

Fig. 2. Experimental apparatus of two dams. (a) Experimental flume from the side. The tempered glass is reinforced by steel joists at intervals of approximately 1.15 m. (b) Upstream and downstream dams.

2.2 Dam material

The grain compositions of the model dams were based on those of the landslide

dams triggered by the Wenchuan earthquake. As shown in Fig. 3, three typical grading curves denoted as fine-grained, well graded, and coarse-grained were derived, corresponding to Donghekou, Tangjiashan and Xiaogangjian landslide dams, respectively (Chang and Zhang., 2010; Chang et al., 2011). The debris types were defined according to the dam materials and differed from the standard engineering classification of soils. The median grain sizes d_{50} of fine-grained and well graded debris were 2.7 mm and 3.7 mm, respectively, which were smaller than the value (20.7 mm) for the coarse-grained debris (Table 1).

The dry densities ρ_d of the experimental dams in all the tests were 1780 kg/m^3: similar to the drillhole data of natural landslide dams (Chang et al., 2011; Zhao et al., 2013). The dam material was prepared by mixing gravel (up to 60 mm), silica sand and silt according to the required grain composition (Fig. S1). After calculation of the total mass of the model dam, the weights of the different fractions were then determined. Finally, the dam materials in different fractions were adequately mixed by repeated stirring.

Geotechnical properties of dam materials were measured. From constant-head permeameter tests (Iverson et al., 2010), the saturated permeability coefficients k of the debris material at the same dry density as the experimental dam were measured (Table 1). The inner diameter of the permeameter was 300 mm to eliminate scale effects with coarse gravel. Coarse-grained debris had a larger permeability coefficient than fine-grained or well graded debris. Large-scale triaxial tests (GCTS, STX-600, 300 mm x 600 mm) were conducted to obtain the shear strengths. The internal friction

angle φ of fine-grained material was smaller than those of coarse-grained and well graded materials.

Table 1. Geotechnical properties of dam materials

Dam material	ρ_d (g/cm^3)	d_{50} (mm)	C_u	C_c	c (Pa)	φ (°)	k (10^{-4} m/s)
Fine-grained	1.78	2.7	5.5	1.2	0	26.8	2.0
Well graded	1.78	3.7	61.3	0.7	0	37.8	3.3
Coarse-grained	1.78	20.7	28.7	2.5	0	43.1	248.0

Note: ρ_d is the dry density of the model dam, d_{50} is the median grain size. C_u and C_c are the uniformity coefficient and curvature coefficient of the grading curve, respectively. c and φ are the cohesion and internal friction angle, respectively. k is the saturated permeability coefficient of dam material.

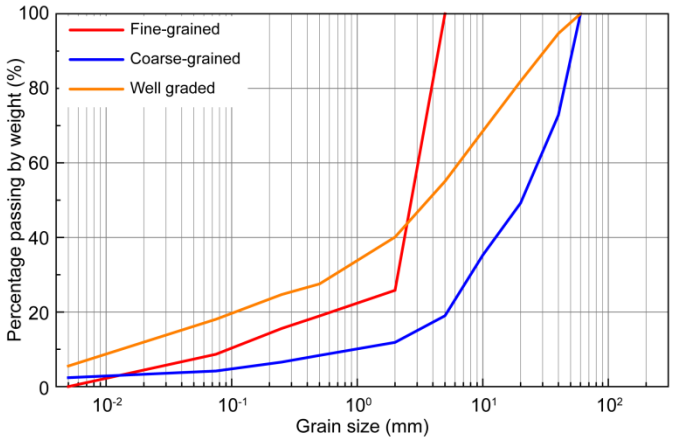

Fig. 3. Grading curves of the experimental model dams.

2.3 Experimental design

The experiments were designed to discern the failure types of single and paired dams, compare the breach processes of dams with different grain compositions and investigate the influence of downstream dams on the amplification effect of cascading

breach discharge. The relevant parameters varied in the experiments were: dam material (fine-grained, well graded and coarse-grained), dam geometry (dam height, crest width) and initial level of impounded water between the upstream and downstream dams (Table 2). In total, three experiments with a single dam and six experiments with two dams were conducted.

Table 2 Characteristics of the different experiments

Test	Upstream dam	Downstream dam			
		Dam material	d_h (m)	d_w (m)	h_w (m)
S1	—	F	0.4	0.3	0
S2	—	W	0.4	0.3	0
S3	—	C	0.4	0.3	0
C1	F	F	0.4	0.3	0
C2	F	W	0.4	0.3	0
C3	F	C	0.4	0.3	0
C4	F	F	0.3	0.3	0
C5	F	F	0.4	0.6	0
C6	F	F	0.4	0.3	0.25

Note: F, C and W represent the fine-grained, coarse-grained and well graded dam materials, respectively. d_h and d_w are the dam height and crest width of the downstream dam (Fig. 1), respectively. h_w is the initial level of impounded water between the upstream and downstream dams.

The grain compositions of the downstream dams in tests C1–C3 varied to match

the corresponding single dam control tests S1–S3. The fine-grained dam in test S1 tended to breach and generate a single-peak outburst flood, compared with the well graded dam in test S2 and coarse-grained dam in test S3. Therefore, the upstream dam was composed of fine-grained debris for all experiments containing two dams. For experiments in which dam geometry or initial water level was investigated (tests C4–C6), fine-grained material was used in the downstream dam.

The geometrical parameters of landslide dams vary widely (Zheng et al., 2021). To study the cascading breach process of landslide dams, this study did not select a specific dam as a prototype. The dams were modeled as trapezoidal prisms of length 0.8 m to match the flume width. The upstream and downstream slopes of the dams were fixed at 30° for all tests, considering the slope of a natural landslide dam is in the range 11–45° (Zheng et al., 2021). The dam height of the upstream dam was 0.90 m (Fig. 1), considering that the height of the experimental flume was 1.25 m. The bottom width along the flume direction was 3.62 m and the crest width was 0.50 m because the ratio of bottom width to dam height of a natural landslide dam is larger than 3.5 (Zheng et al., 2021). For the downstream dam, the bottom width was 1.69 m, the crest width was 0.30 m, and the dam height was 0.40 m for tests S1–S3, C1–C3 and C6. The dam height was reduced to 0.3 m (bottom width 1.34 m) for test C4 and the crest width was increased to 0.6 m (bottom width 1.99 m) for test C5. A rectangular slot with a depth and width of 0.05 m was located in the middle of each dam to simulate the artificial spillway that is often constructed in a landslide dam in an effort to reduce breach discharge. The inflow rate was determined to be 1.13 L/s

based on geometric scaling (nearly 1:100) and Froude scaling of the inflow rate (113 m^3/s) of the Tangjiashan landslide dam (Peng et al., 2014).

The initial level of impounded water between the upstream and downstream dams was 0.25 m in test C6 only, while it was zero in all other tests. The distance between the upstream and downstream dams was 10.00 m for all of the tests (Fig. 1). The single dams were located in the same position as the downstream dams in the tests of cascading failure.

2.4 Experimental procedure

The experimental procedure contained five stages:

(1) Experimental preparation. An outline and grids were drawn on the sidewall of the flume with a grease pencil, according to the shape of the predesigned dams in the upstream and downstream.

(2) Dam construction. Dams were formed by depositing debris in layers of 10 cm thickness. Each layer was uniformly compacted by slightly tapping with a steel trowel to obtain the required dry density before adding the next layer. After a dam had been constructed, a rectangular slot was excavated on the surface of the dam crest.

(3) Data record. Video and still cameras were installed in their specified positions. During each test, the images and videos collected by the cameras were auto-saved on a computer.

(4) Water inpouring. The inflow rate was maintained at 1.13 L/s for all tests by means of an electromagnetic flowmeter. The dewatering pump operated at maximum power during the whole breach process to discharge the seepage water passing

through the single or downstream dam. If the landslide dam remained stable for more than 2 hours after the upstream water level reached its maximum, as in test S3, the inflow rate was doubled to 2.26 L/s to induce failure of the dam.

(5) Data processing. The failure type for each dam was discerned from the recorded snapshots. The stage hydrographs of single and paired dams were calculated. The breach discharge q_b was calculated from the upstream stage hydrograph of the dam.

$$A_l \frac{dH_t}{dt} = q_{in} - q_b - q_s \tag{1}$$

where A_l is the surface area of lake water and H_t is the upstream water level. q_{in} is the inflow rate to the upstream reservoir of the dam. q_s is the seepage discharge, calculated using H_t (Fig. S2). q_b and q_s of the upstream dam was regarded as q_{in} of the downstream dam.

The stage hydrograph of the downstream dam may fluctuate, as in test C6. It was measured in four positions and the water level H_t was the average value of all the measured water levels,

$$H_t = \sum_{1}^{4} H_{ti} / 4 \tag{2}$$

where H_{ti} is the water level at each of the four measuring points.

3. Failure types and breach processes of landslide dams

In this section, the failure types of single fine-grained, well graded and coarse-grained dams (tests S1–S3) are first compared with downstream dams composed of the same dam material (tests C1–C3). Then, breach processes of

downstream dams with different grain compositions (tests C1–C3) are analyzed. Finally, the peak breach discharges of single dams and downstream dams (tests S1–S3 and C1–C3) are discussed.

3.1 Failure types of landslide dams

For the fine-grained dam in test S1, the water seeped through the dam body near the toe of the downstream face when the upstream water level H_t reached 5.2 cm. The debris at the dam toe was first carried away as the upstream water level H_t reached 11 cm (Fig. 4a). The downstream dam slope under the seepage line was gradually eroded because the sum of the seepage stress and sliding stress generated by gravity was larger than the shear strength of fine-grained debris (Table 1). The downstream dam slope above the seepage line collapsed and this caused a near-vertical free face above the seepage line (Fig. 4a). The width of the dam crest decreased due to the seepage instability of the downstream slope face of the dam when the near-vertical free face reached the dam crest. This seepage played a major role in the stability of the downstream dam slope before overtopping. Subsequently, the water in the upstream reservoir overflowed through the slot and an overtopping failure was initiated. The breach rapidly broadened in both the stream flow and cross-stream directions because part of the dam crest had been eroded by the seepage instability.

A similar free face developed on the downstream slope face of the downstream dam in test C1. However, this near-vertical free face did not reach the dam crest and the dam crest remained stable when the outburst flood of the upstream dam was released (Fig. 4b). Seepage was essentially irrelevant to the dam's failure. The height

of the near-vertical free face was smaller than that of the single dam in test S1. This is because the downstream dam had a lower upstream water level (28 cm) and limited time to develop the near-vertical free face before breaching of the upstream dam. The upstream water level of the downstream dam rapidly increased and the dam crest was eroded by the turbulent flood after the upstream dam breached. The breaching floods of upstream and downstream dams were combined at the downstream dam site. The maximum water depth during the breach process was 45 cm, which was larger than the values for the single dam in test S1 (38 cm) and the dam height. The time from the beginning of overflow to the end of dam breaching (62 s) was shorter than the value for test S1 (128 s). The end of dam breaching was taken as the time when the dam was no longer eroded by the overflow. The overtopping failure of the downstream dam was induced by the outburst flood of the upstream dam. By contrast, the single dam with fine-grained debris (test S1) failed by overtopping along with seepage instability. The upstream dam composed of fine-grained debris in the cascading test C1 followed a similar failure process to test S1.

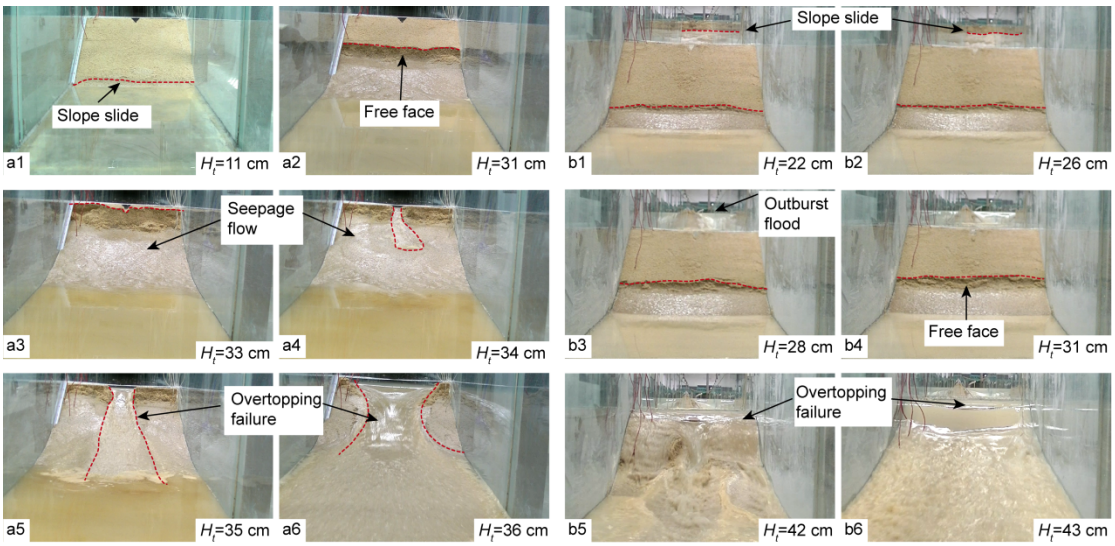

Fig. 4. Breach processes of dams with fine-grained debris material: (a) single dam (test S1) and (b) two dams (test C1). Single dams with fine-grained debris failed by overtopping along with seepage instability; a downstream dam with the same dam material failed by overtopping alone.

As shown in Fig. 5, when water propagated through the slot of a single dam with well graded debris (test S2), headcutting was generated by exceeding the critical shear stress for incipient sediment movement on some part of the dam's downstream face. This headcutting was not observed in test S1 because the fine-grained debris had a lower shear strength and hence a greater tendency to be carried away by the overflow compared with well graded debris (Table 1). A channelized flow then formed which, in turn, broadened the width and depth of the channel due to a large slope (30°). This positive feedback mechanism increased the channelized discharge, with a consequent removal of superficial debris grains and a progressive migration of the channel head toward the dam crest. Some coarse sediment was deposited near the toe of the downstream slope and the channel was gradually deflected. Finer grains were easier to wash away than coarse grains as a result of a large uniformity coefficient of grain composition, contributing to the formation of a step-pool structure (Wang et al., 2012). Side slope collapse occurred as the channel head reached the upstream face of the dam. The time from the beginning of overflow to the end of dam breaching (197 s) was longer than the value for test S1 due to the migration of the headcutting. The channel shape along the stream was similar to an hourglass and it was close to trapezoidal in the cross-stream direction. This breach process was consistent with the observations of the Tangjiashan landslide dam (Chang and Zhang, 2010).

For the downstream dam in test C2, fine grains under the seepage line were carried away by the seepage initially, which was similar to the observation in test S2. The toe of the downstream slope remained stable due to the low hydraulic gradient and high shear strength (Table 1). When the upstream dam began breaching, the upstream water depth of the downstream dam was 16 cm in test C2: smaller than the equivalent value for the downstream dam in test C1 (28 cm). This difference was due to a larger permeability coefficient of well graded debris causing more seepage through the downstream dam. The time from the beginning of overflow to the end of dam breaching (66 s) was shorter than the value for test S2. The dam crest was directly eroded by the overflow in test C2, while the dam crest remained stable during headcutting migration on the downstream slope of the dam in test S2. A step-pool structure was also generated by the overtopping flow from the upstream dam as for test S2. The step-pool structure was confined to the channel in test S2 but it occupied the whole flume width in test C2 due to the large outburst discharge of the upstream dam. This step-pool structure is consistent with the observations of the Tiger-leaping Gorge and Yujunmen landslide dams (Wang et al., 2009; Wang et al., 2012). The failure type of the downstream dam in test C2 was overtopping because of the large outburst flood from the upstream dam. By contrast, the single dam in test S2 failed by headcutting due to a small inflow rate.

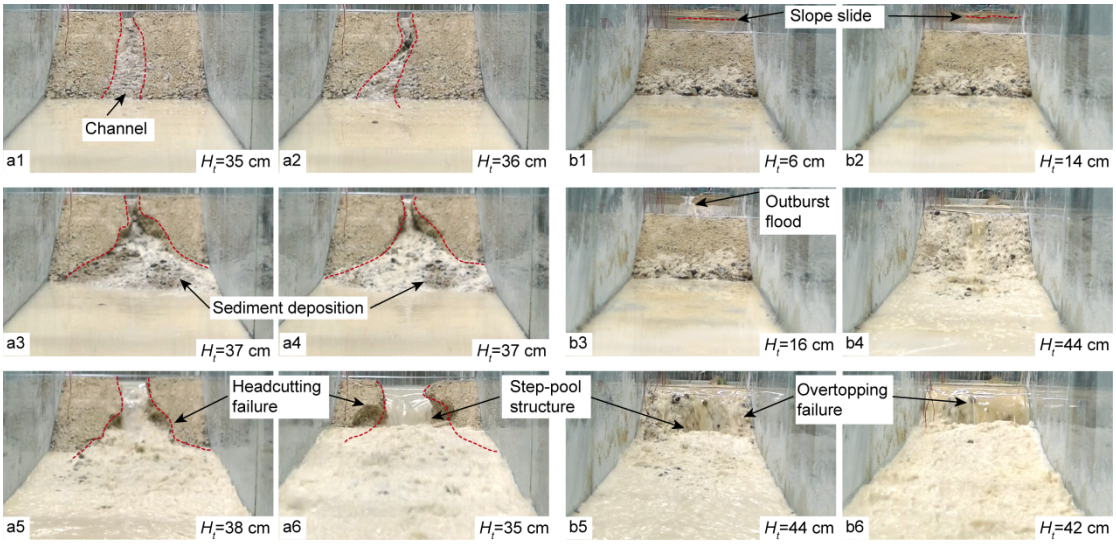

Fig. 5. Breach processes of dams with well graded debris: (a) single dam (test S2) and (b) two dams (test C2). The single dam failed by headcutting. The downstream dam in the cascading test with well graded debris failed by overtopping.

As shown in Fig. 6, the upstream water depth of a single dam in test S3 slowly increased because the material's high seepage coefficient produced a high seepage flow through the dam (Table 1). After water flowed through the dam crest, fines on the downstream slope face were taken away and the dam remained stable for more than 2 hours. The outflow water gradually became transparent, indicating that few grains were being washed away. The channelizing and headcutting did not occur on the downstream slope due to the high shear strength of coarse grains. After the inflow rate was doubled, an overtopping failure developed because the shear stress exerted by the overflow was large enough to erode coarse grains.

The water depth of the downstream dam in test C3 was 14 cm upon breaching of the upstream dam, which was smaller than the values for downstream dams composed of fine-grained or well graded debris (tests C1 or C2, respectively). Then the water depth rapidly increased and part of the downstream slope slid because abundant water

seeped out from the downstream slope surface (Fig. 6). The coarse grains tended to be eroded by the outburst flood from the upstream dam (peak flow rate reached ~60 L/s) and an overtopping failure was induced. The time from the beginning of overflow to the end of dam breaching (64 s) was almost the same as those for tests C1 and C2 because debris grains of different sizes can be transported by the large outburst flood from an upstream dam. The downstream dam with coarse-grained debris failed by overtopping, which was consistent with the single dam in test S3.

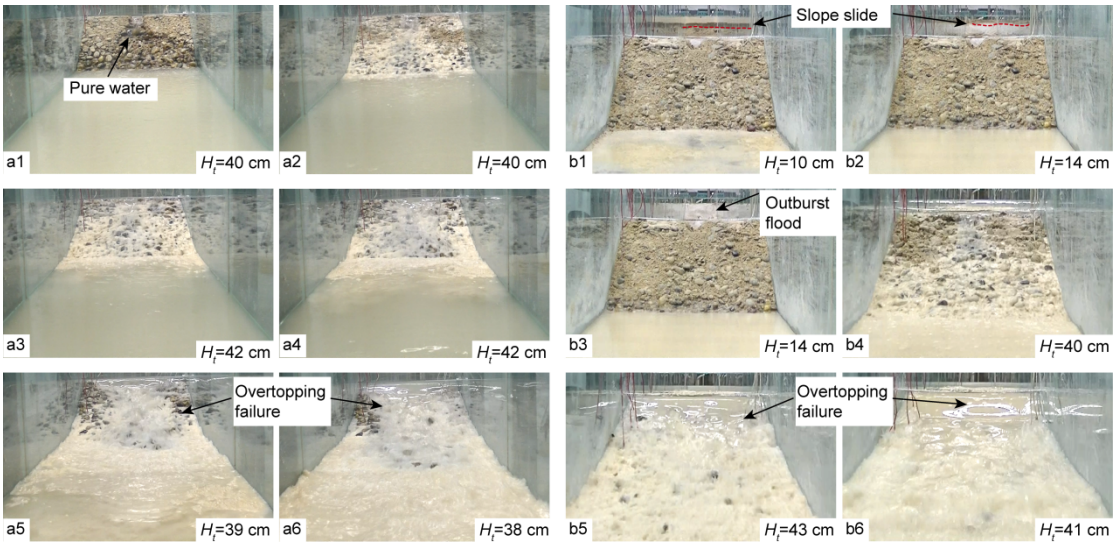

Fig. 6. Breach processes of dams with coarse-grained debris : (a) single dam (test S3) and (b) two dams (test C3). Both the single dam and the downstream dam in the cascading test with coarse-grained debris failed by overtopping. The single dam with coarse-grained debris remained stable when the inflow rate was 1.13 L/s; it failed by overtopping when the inflow rate was doubled (Fig. 6a2).

3.2 Breach processes of landslide dams

3.2.1 Comparison between the two dams

Breach processes of downstream dams with different grain compositions differed,

even though all failed by overtopping. For fine-grained dams, the slope of the downstream side was 30°, although the slope toe failed due to the seepage. Subsequently, the downstream slope angle rapidly decreased because the dam material was transported downstream by the overtopping flow. Then a flat angle in the range 14.4–16.2° was sustained during the breach (Figs. 7a and S3). This failure process is consistent with the theoretical model proposed by Powledge et al. (1989).

A step-pool structure was first developed for well graded landslide dams because the finer grains on the downstream dam slope were easier to wash away than the coarser grains as a result of a large uniformity coefficient of grain composition (Figs. 7b and S4). The step-pool structure migrated toward the dam crest and the height of the step gradually increased. After dam breaching, the fine debris grains on the surface of the residual dam were carried away by the overtopping flow leaving the coarser grains undisturbed, contributing to the formation of an armoring layer (Fig. S6).

The downstream slope angle quickly decreased by the overflow for a downstream coarse-grained dam and this angle persisted during the breach (Figs. 7c and S5). This was similar to the failure process of the fine-grained dam in the downstream. The downstream slope angle ranged from 7.4–10.4° which was smaller than the value for the fine-grained dam in the downstream. The reason was that some of the coarse debris grains transported by the outburst flood were deposited close to the dam site.

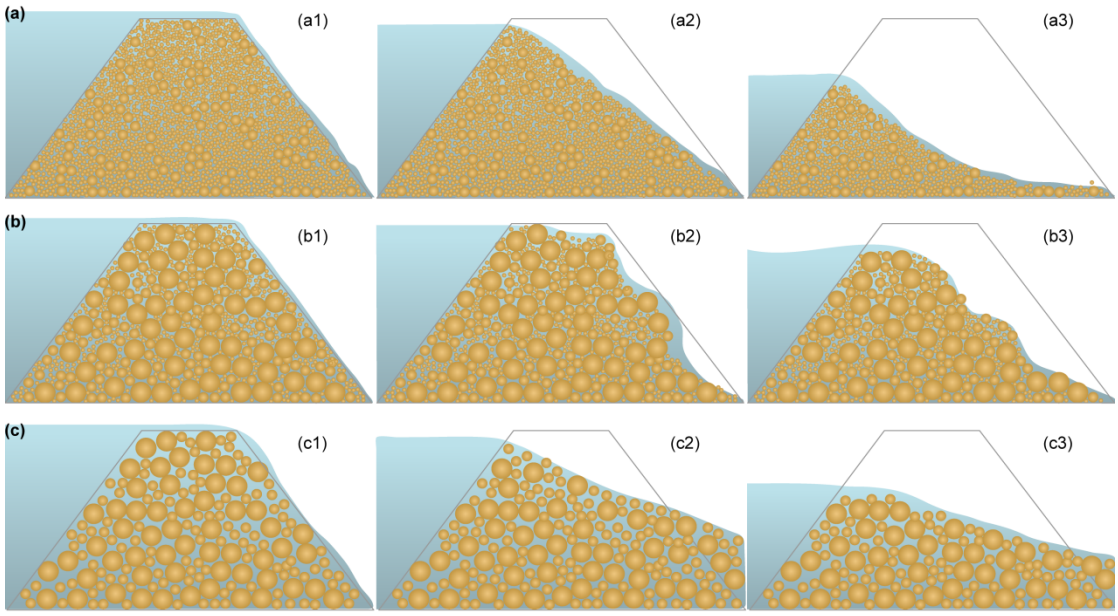

Fig. 7. Breach processes of landslide dams downstream in tests C1–C3. (a), (b) and (c) denote fine-grained, well graded and coarse-grained dams, respectively.

The durations of the breach processes were almost the same for tests C1–C3, although the breach processes differed depending on dam material. Briaud (2008) estimated the critical velocity for grain initiation of the debris materials presented here to be 0.6–1.3 m/s based on the mean grain diameter. The flow velocities of downstream dams during the breach processes were estimated to be 1.4–1.8 m/s based on the breach discharge and flow depth. The debris grains with different sizes tended to be carried away by the outburst flood from the upstream dam.

3.2.2 Comparison between single and cascading dams

The peak breach discharges of a single dam with different grain compositions (tests S1–S3) were less than 16 L/s (Fig. S7). The peak breach discharges of downstream dams (tests C1–C3) were more than 6 times those of the corresponding single dams due to the outburst floods from the upstream dams. The breach processes

of the upstream and downstream dams overlapped (Figs. 4–6) and the breach discharge of an upstream dam was a part of the breach discharge of a downstream dam. Moreover, the breach rate of a downstream dam was enhanced compared with a single dam which, in turn, fortified the breach discharge.

Seepage through a downstream dam slope had a substantial effect on the breach process. As shown in Fig. 8, the seepage lines of single and downstream dams migrated from the dam base to the dam crest with the increase of upstream water depth. At the initial impounding stage, the seepage lines were basically parallel to each other with a gradient of 4–7° to the horizontal. Then the seepage lines of single dams slightly steepened as a result of the increase of water depth and decrease of infiltration length. By contrast, the gradients of seepage lines of downstream dams increased to 14–20°, due to a rapidly rising water level. Considering the seepage stress reduced the stability of a downstream dam slope and accelerated the breach process, a simplified calculation was made to evaluate the effect of seepage stress f_s on the stability coefficient s of a downstream dam slope (Fig. S8).

$$s = \frac{R_s}{F_s + f_s} \tag{3}$$

where F_s is the sliding stress generated by gravity. R_s is the resistance stress

$$R_s = c + \sigma \tan\varphi \tag{4}$$

where σ is the effective normal stress. F_s is expressed as

$$F_s = \rho_d g h \sin\alpha \tag{5}$$

where h is the slide thickness, g is gravitational acceleration and α is the slope angle. The seepage stress f_s is expressed as

$$f_s = \rho_w g h i \tag{6}$$

where i is the hydraulic gradient and ρ_w is the water density. For example, for a dam of well graded debris and a downstream slope angle α = 15° during the breach, the stability coefficient s decreases from 1.92 to 1.07 with i increasing from 0 to 0.36.

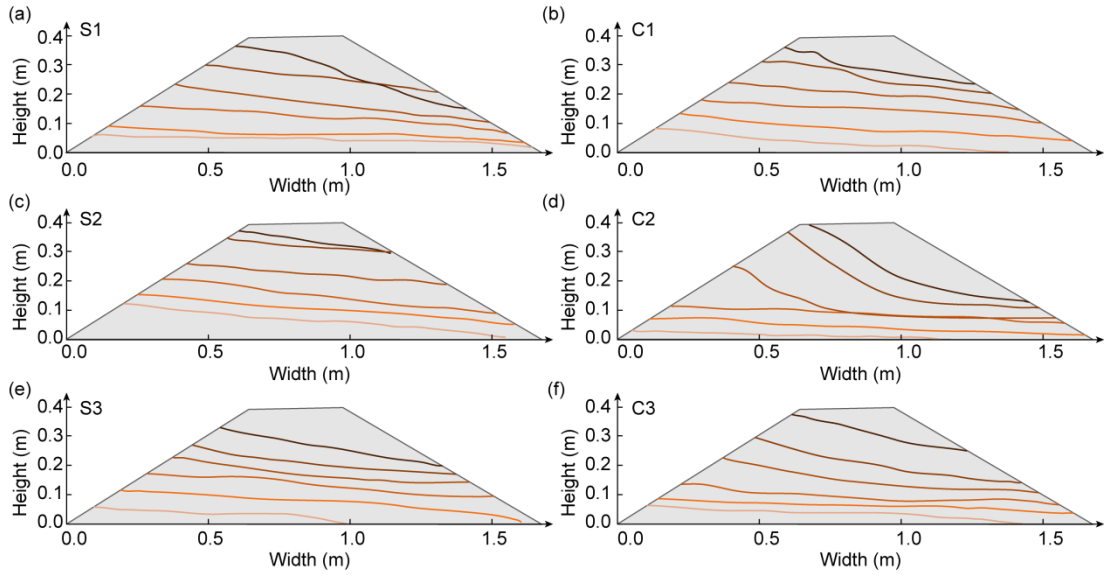

Fig. 8. Evolution of seepage lines of tests S1–S3 and C1–C3. The seepage lines intersect in test S1 due to the downstream slope instability of the dam with fine-grained debris.

4. Amplification effect of cascading breach discharge of landslide dams

4.1 Effects of grain composition on the cascading breach

Discharge hydrographs of the upstream and downstream dams in tests C1–C3 are shown in Fig. 9. The breach discharge of each downstream dam rapidly increased and then gradually declined to match the discharge of the upstream dam. The amplification factor of the peak discharge A_f is defined as

$$A_f = q_d / q_u \tag{7}$$

where q_u and q_d are the peak discharges of the upstream and downstream dams,

respectively. A_f was larger than 1.6 for various grain compositions. The amplification effect of breach discharge occurred after the cascading breach of two dams, although the downstream dams had smaller dam volumes.

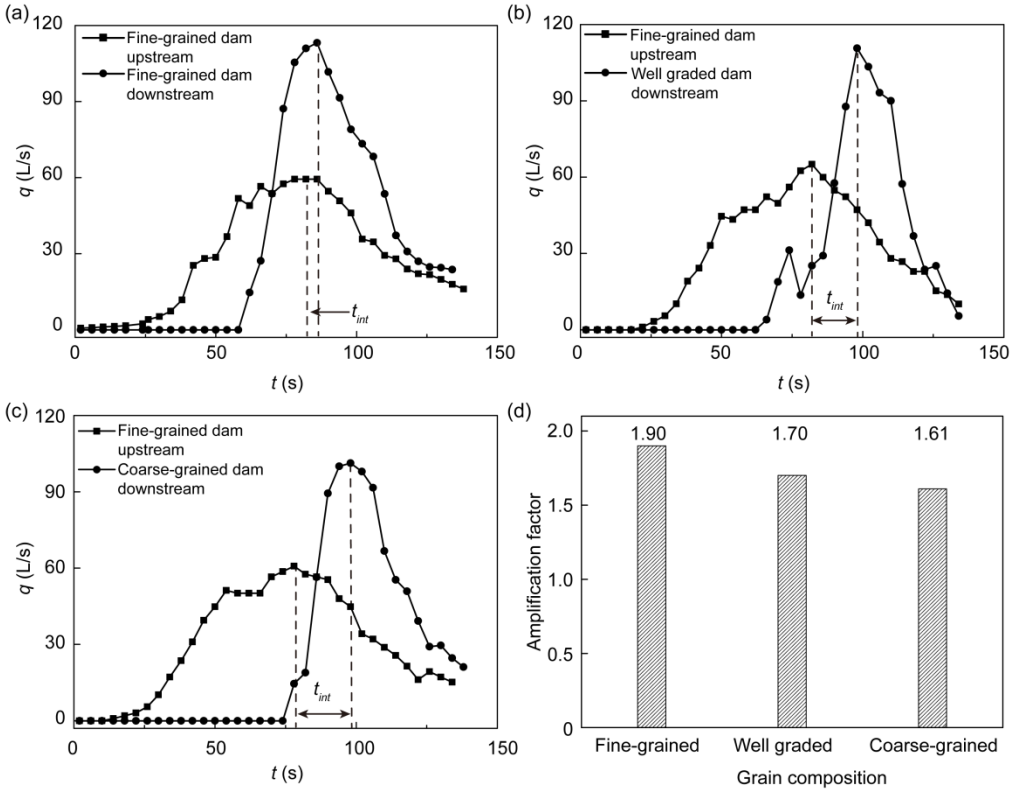

Fig. 9. Discharge hydrographs of landslide dams. (a), (b) and (c) Discharge hydrographs of the upstream and downstream dams in tests C1, C2 and C3, respectively. (d) Amplification factor A_f of the peak discharge for different grain compositions.

For test C1, the peak breach discharge of the downstream dam was amplified to 113 L/s, representing a 90% increase of the upstream peak breach discharge (Figs. 9a and 9d). The time t_{bo} from the breach of the upstream dam to overflow of the downstream dam was only 26 s. This was due to a low permeability coefficient of the downstream dam causing a low seepage flow and a high water depth (28 cm). The large outflow flowed through the slot and dam crest of the downstream dam at the

same time (Fig. S3). As a result of the low shear strength of fine-grained material and seepage stress (Fig. 8), the downstream slope of the downstream dam was rapidly incised and a complete dam breach (i.e., when the width of the dam crest decreased to zero) developed within 5 s (Fig. 4). The time interval t_{int} between peak breach discharges of the two dams was only 5 s, indicating that the overlapping effect of breach discharges of the fine-grained dams was considerable.

For tests C2 and C3, the peak breach discharges were amplified to 110 L/s and 98 L/s, respectively, representing increases of 70% and 61% on the corresponding upstream peak breach discharges (Figs. 9b–9d). Two peaks successively occurred in the discharge hydrograph for test C2 due to the step-pool structure. The first peak (31 L/s) at 74 s was caused by the breach from the upstream dam; the second peak (110 L/s) at 98 s was induced by the breach from the downstream dam.

The amplification effects of cascading breach discharges of well graded and coarse-grained dams were relatively limited compared with the fine-grained dam. The t_{bo} for tests C2 and C3 were 36 and 52 s, respectively, which were larger than the value in test C1. This is because the higher permeability coefficients of downstream dams in tests C2 and C3 compared to test C1 led to a larger seepage flow and a lower upstream water level. The breaches of downstream dams in tests C2 and C3 were delayed compared with test C1. Before the outburst flood flowed through the well graded and coarse-grained dams, the downstream slopes of both dams were slightly eroded due to their high shear strength. Approximately 15 s elapsed from the beginning of overflow to complete dam breach which was longer than for the

fine-grained dam (5 s). The t_{int} between peak discharges of the two dams were 16 s and 20 s for well graded and coarse-grained debris, respectively: larger than for the fine-grained dam. When the peak breach discharge of the downstream dam occurred, the breach discharge of the upstream dam declined and the amplification effect of cascading breach discharge was reduced.

4.2 Effects of dam geometry on the cascading breach

Test C4 was the same as test C1 except the height of the downstream dam in test C4 was 0.3 m while it was 0.4 m in test C1. The peak discharge of the downstream dam in test C4 was amplified to 99 L/s: an increase of 46% on the upstream peak discharge. The peak discharge and amplification effect of the two dams in test C4 were smaller than those of test C1. The reason is that the highest upstream water level of the downstream dam in test C4 was 39.5 cm and the maximum lake volume during the breach process was smaller than that of test C1. The cascading breach discharge produced by the downstream dam was relatively limited. In addition, due to a smaller dam height, the t_{bo} was 24 s and the downstream dam had breached before the peak discharge of the upstream dam occurred. This is similar to the observations of the Tangjiashan and Xinjiecun landslide dams (Peng et al., 2014). The time interval t_{int} between peak discharges of the two dams in test C4 was 22 s: considerably longer than for test C1 (5 s). Therefore, the two dams in test C4 had a smaller amplification effect than for test C1.

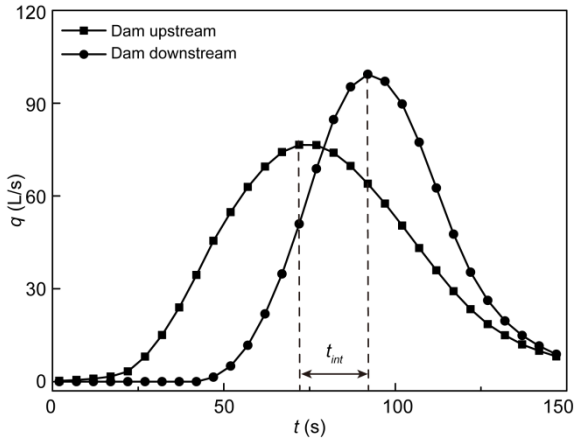

Fig. 10. Discharge hydrographs of the two dams in test C4.

Test C5 was the same as test C1 except the crest width of the downstream dam in test C5 was 0.6 m while it was 0.3 m in test C1. The peak breach discharge was amplified to 96 L/s: an increase of more than 41% on the upstream peak breach discharge (Fig. 11). Two peaks successively occurred in the discharge hydrograph of the downstream dam. The first peak (96 L/s) at 82 s was generated because the downstream dam had been breached by the outburst flood. The second peak (86 L/s) at 102 s was preceded by the second peak of the upstream dam (at 92 s). The peak breach discharge and its amplification effect in test C5 were smaller than those of test C1. The reason is that due to a larger dam crest, the time from the beginning of overflow to complete dam breach in test C5 was prolonged and persisted for about 15 s, while it was approximately 5 s for test C1. The t_{int} of the two dams was 26 s: longer than for test C1. The breach processes of the two dams in test C5 were highly separated and the amplification effect of the cascading breach discharge was thus reduced.

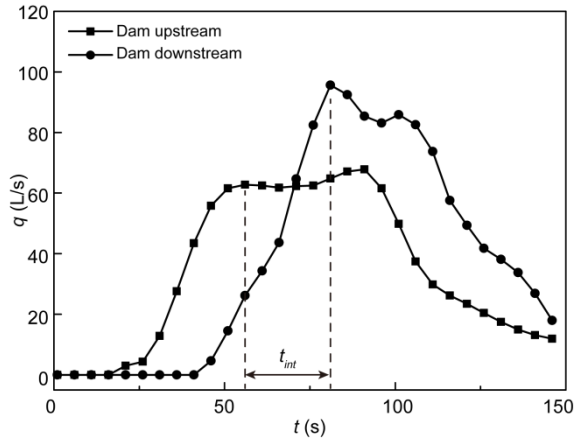

Fig. 11. Discharge hydrographs of the two dams in test C5. Considering that the upstream dam had completely breached before the first peak (t = 56 s), the time interval between the peak discharges of the upstream and downstream dams was determined to be 26 s.

4.3 Effects of water level on the cascading breach

Test C6 was the same as test C1 except the initial level of impounded water between the upstream and downstream dams in test C6 was 0.25 m while it was zero in test C1. The peak breach discharge was amplified to 112 L/s: an increase of approximately 60% on the upstream breach discharge (Fig. 12). The t_{bo} was only 11 s and the breach of downstream dam was advanced, compared with test C1. The combined initial water level and flood wave induced a surge wave (Fig. 13). After the surge wave passed through the dam crest, the downstream dam slope and dam crest were strongly eroded and partially collapsed as a result of the low shear strength of fine-grained material and high hydraulic gradient. The width of the dam crest was reduced by the surge wave and the breach process proceeded before the peak discharge of the upstream dam occurred. The t_{int} of the two dams in test C6 was 21 s which was longer than for test C1. Therefore, the two dams in test C6 had a smaller

amplification effect than those for test C1.

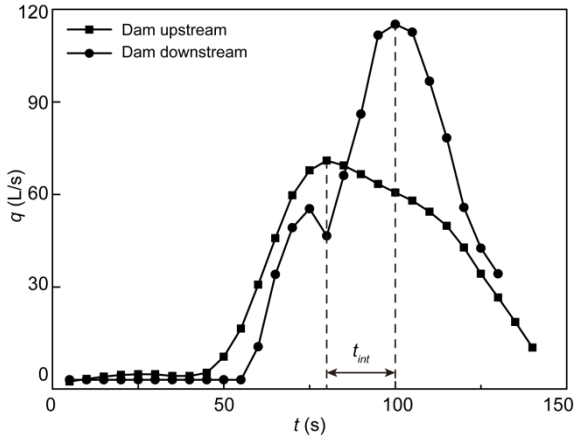

Fig. 12. Discharge hydrographs of the two dams in test C6.

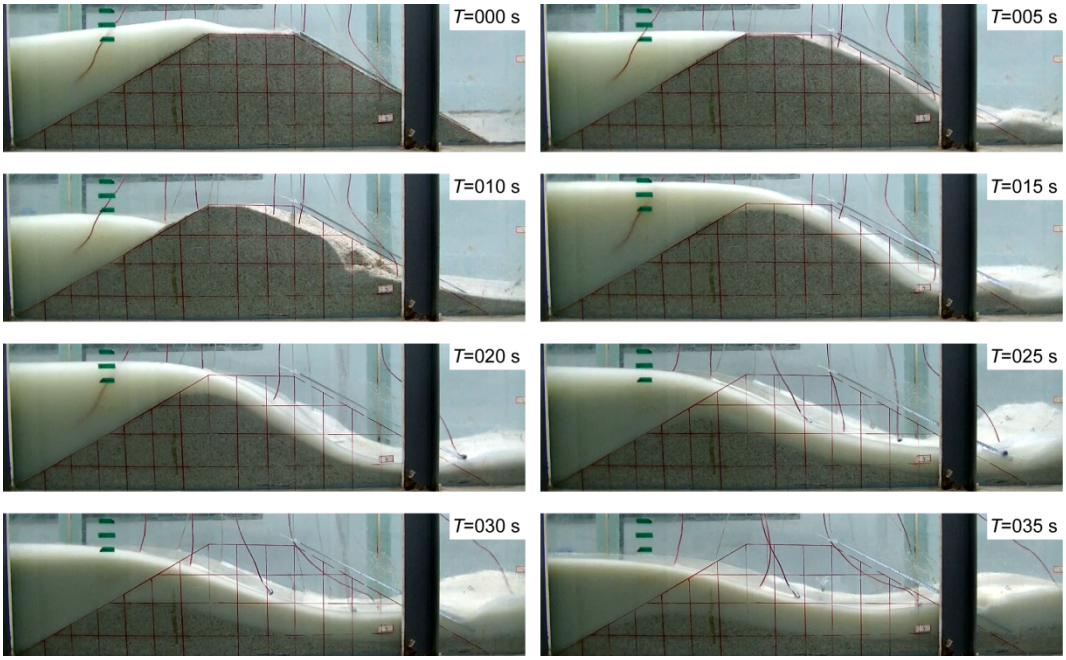

Fig. 13. Cascading breach process of fine-grained landslide dams with an initial impounded water level of 25 cm (test C6). *T* is the time elapsed when overtopping flow propagated through the guiding slot.

4.4 Amplification effect of the cascading breach

The breach processes of the two dams lasted from the breach of the upstream dam to overflow of the downstream dam and the breach of the downstream dam.

Considering the overlap of breach processes, the time interval t_{int} between the peak discharges of the two dams was correlated with the amplification factor A_f as shown in Fig. 14. The correlation between A_f and t_{int} was highly linear (determination coefficient R^2=0.92) for various cases,

$$A_f = at_{int} + b \tag{8}$$

where a and b are the slope (-0.02) and intercept (2.05), respectively. As the time interval increased, the breach processes for the upstream and downstream dams gradually separated and thus the amplification effect was reduced.

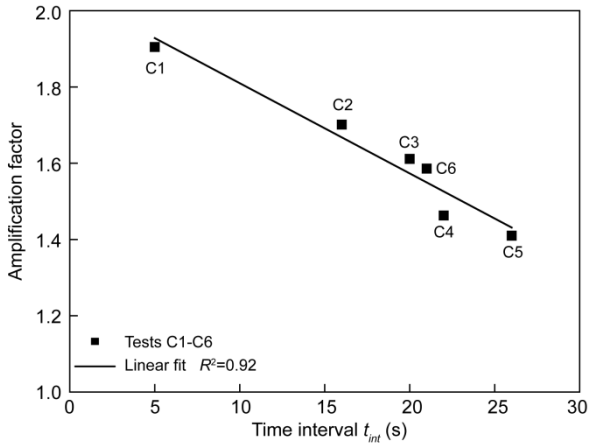

Fig. 14. Amplification factor A_f against the time interval t_{int} between peak discharges of the two dams in tests C1–C6. The amplification factor had a negative linear correlation with the time interval between the peak discharges of the two dams. R^2 is the determination coefficient.

5. Discussion

5.1 Failure types of landslide dams

Single dams fail by overtopping along with seepage instability for a fine-grained dam, headcutting for a well graded dam and overtopping for a coarse-grained dam, respectively, due to a slowly rising water level in these dams with large storage

capacities. The failure type is influenced by the seepage coefficient and shear strength of the dam material for a single dam in our experiments. However, downstream dams invariably fail by overtopping, irrespective of grain composition, due to the large outburst floods from the upstream dams.

Experimental observations of Chen et al. (2015) indicate that single dams with high permeability coefficients fail by overtopping along with seepage instability. However, this failure type occurred for the single fine-grained dam with a low permeability coefficient in our experiments. The explanation is the permeability coefficients in the experiments of Chen et al. (2015) are limited to 2.3×10^{-5} cm/s, which is smaller than the value for fine-grained debris (Table 1) in our experiments.

According to the model reported by Powledge et al. (1989), the downstream slope angle of a landslide dam rapidly changes until a constant critical soil friction angle is achieved during the breach process, after which the angle is maintained to the end of breaching. This model is consistent with the observations of the fine-grained and coarse-grained dams. However, the angle for the fine-grained dam is 14.4–16.2° which is lower than the critical soil friction angle of 26.8° based on the equilibrium of energy loss (Powledge et al., 1989). The reason for the difference may be that the effect of seepage on the downstream dam slope (Equations 3–6) is not considered in the model proposed by Powledge et al. (1989). In addition, the constant angle (7.4–10.4°) for the coarse-grained dam is lower than the value of the critical soil friction angle (43.1°). Compared with the fine-grained dam, the debris grains in the coarse-grained dam are transported by the breach flood and are more likely to deposit

close to the dam site (Figs. S5 and S6). The downstream slope of the dam is thus reduced.

5.2 Amplification effect of cascading landslide dams

The experimental results show that the condition for the amplification effect of the cascading breach discharge of two dams is that the breach processes of the upstream and downstream dams overlap. For example, the peak breach discharge of the Xiaogangjian landslide dam, with a dam height of 30 m and a dam volume of 2×10^6 m^3, was 2251 m^3/s (Chen et al., 2018). The peak discharges were amplified to 2515 m^3/s and 3329 m^3/s after the breaching flood flowed through the Xiaogangjian and Yibadao landslide dams further downstream. However, if the breach processes of multiple landslide dams are completely separated, there may be very little measurable effect of amplification effects of cascading breaching (Shi et al., 2015). For example, Xinjiecun landslide dam, located downstream of the Kuzhuba dam, was completely destroyed by the breaching flood from the Tangjiashan landslide dam. The recorded peak breach discharge in Xinjiecun was just 6540 m^3/s (Peng et al., 2014), which was slightly larger than the value for the Tangjiashan landslide dam (6500 m^3/s). The reason is that the breach initiation for the Tangjiashan landslide dam lasted for 71 hours and the Kuzhuba and Xinjiecun landslide dams had completely breached as a result of their small lake volumes before the arrival of the peak breach discharge from the Tangjiashan landslide dam.

The cascading peak discharges in our experiments are larger than the sums of the peak discharges of upstream and single dams by comparing tests C1 and S1, tests C2

and S2, and tests C3 and S3. This is different from the prediction of Shi et al. (2015) that the maximum cascading peak discharge is equal to the sum of the peak discharges of upstream and single landslide dams when the time interval between peak breach discharges of two landslide dams is zero. The upstream water level of the downstream landslide dam rose quickly and applied a considerable seepage stress to the dam (Fig. 8), contributing to rapid breaching of the downstream dam. In addition, the outflow from the upstream landslide dam has a flow velocity along the river channel and breach incision of the downstream landslide dam is enhanced due to a larger erosion stress. These physical processes are not considered in the DABA breach model (Shi et al., 2015).

5.3 Multiple peaks and surge waves

Multiple peaks in a discharge hydrograph may be generated by different factors. For test C2, the first peak with a smaller magnitude is caused by the breach discharge from the upstream dam (Fig. 9), while the second peak with a higher magnitude is induced by the cascading breach discharge from the downstream dam. Thus, the two peaks occur successively. Affected by the surge wave, two peaks of breach discharge are generated in test C6 (Fig. 13). Multiple peaks generated by upstream and downstream dams can be predicted by a physically-based breach model (Shi et al., 2015).

For a single dam in test S2, the discharge hydrograph also has multiple peaks (Fig. S7). The primary reason is that a step-pool structure is formed during the breach of a well graded dam. When the finer grains on the bottom of the breach are washed

away and the coarse grains are left behind, the outflow increases first and then decreases, resulting in a peak in the discharge hydrograph. When the coarser grains are scattered and pushed away, the overflow continues to incise the breach and later another peak discharge occurs.

Commonly, a surge wave is formed when a landslide, avalanche or debris flow with a high flow velocity slides into a lake with a huge volume (Fritz et al., 2004; Xu et al., 2015). For example, a landslide of 300 million m^3 rapidly slid into the Vaiont Reservoir in Italy in 1963, causing enormous surge run-up heights of approximately 230–250 m at the opposite shore (Semenza and Ghirotti, 2000). A glacial avalanche with a volume of 6.5 million m^3 rushed into a moraine lake in Nastetuku River, Canada, in 1983 and the moraine dam was completely breached in less than 5 hours under the impact of large surge waves (Risley et al., 2006). A surge wave was also developed in our experiments (test C6) when the breach discharge from the upstream dam rushed into the downstream river. The surge wave can reduce the dam height and accelerate the breach process of a downstream dam (Peng et al., 2019).

5.4 Geometrical characteristics of residual dams

Regardless of single or paired dams, the maximum residual dam height h_r and slope θ along the flume increase with increasing shear strength of the debris materials (Figs. 15 and S6). h_r of a single dam with fine-grained debris is 12 cm and the residual slope is nearly horizontal. These values are lower than the corresponding values for dams composed of well graded or coarse-grained debris. The reason is that as the proportion of fine grains increases, the dam material, especially in the upstream slope

of the dam, becomes more likely to be eroded by a breach flood contributing to a smaller residual slope. h_r and θ of a single dam are smaller than those of a downstream dam in a cascading test for the same grain composition, although a single dam has a smaller peak breach discharge than paired dams. Dam material with different grain sizes is eroded away by the outburst flood because the flow velocity during the breach is higher than the estimated critical velocity for grain initiation (Briaud, 2008). The breach processes last 62–66 s for the downstream dams (Fig. 9) and are shorter than those (~100 s) of the single dams. Due to a longer breaching process, much more material from single dams was transported downstream than from downstream dams in a paired configuration. In addition, part of the lake volume was retained by the upstream residual dam with a height of nearly 0.45 m, thus reducing the volume of the breaching flood from the upstream dam to erode the downstream dam.

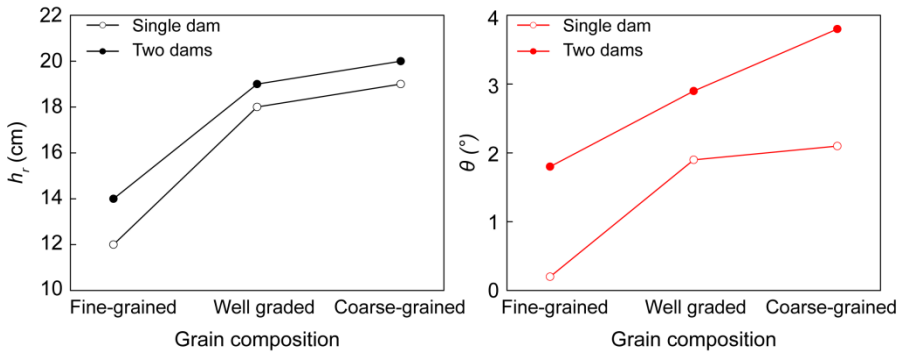

Fig. 15. Residual dam height h_r and slope θ (°) of single and paired dams.

6. Conclusions

We compared the breach processes of single and paired dams through a series of experiments by considering grain compositions and dam geometry. In particular, we

discerned the failure type and quantitatively evaluated the amplification effect of cascading breach discharge of two dams.

(1) The type of failure of a single dam varies with grain composition and is influenced by the shear strength and seepage coefficient of the dam material. By contrast, downstream dams fail by overtopping, irrespective of grain composition. A general stable angle is maintained during the breach for the fine-grained and coarse-grained dams, while a step-pool structure is developed for the well graded dam.

(2) The amplification effect of breach discharge occurred after the cascading breach of two dams due to the outburst flood of the upstream dam. Compared with coarse-grained and well graded dams, breach processes of the downstream dam with fine-grained material were highly overlapped with the upstream dam, resulting in a larger peak breach discharge and amplification effect. The amplification effect of cascading dams was reduced by a smaller dam height or a larger dam crest. The amplification effect linearly decreases with increasing time interval between peak breach discharges of the two dams for various cases.

(3) Multiple peaks in a discharge hydrograph may be generated by cascading failure from upstream and downstream dams, the formation of a step-pool structure for well graded dams, or surge waves.

(4) The residual dam heights and slopes along the flume of single and paired dams increase with increasing shear strength of the debris materials. Due to a longer breach process and a larger volume of breaching flood for a single dam, the residual

dam height and slope of a single dam are smaller than those of a downstream dam in a cascading test for the same grain composition.

The experiments show that the breach process and discharge of multiple dams are different from those of a single dam, creating a great challenge to predict the outburst flood from multiple dams. These experimental results can provide calibration for numerical simulations of breach processes of single and paired dams.

Acknowledgements

We acknowledge funding from the Natural Science Foundation of China (No. 41731283, 41877234, 42007252 and 42061160480). Constructive reviews by the editor and two anonymous reviewers helped to improve the manuscript and are gratefully acknowledged.

Conflicts of Interests

The authors declare that they do not have any conflict of interest.

Notation

A_f amplification factor of the peak discharge

A_l surface area of lake water

C cohesion of dam material

C_c curvature coefficient of the grading curve

C_u uniformity coefficient of the grading curve

d_{50} median grain size of a dam material

d_h height of a downstream dam

d_w crest width of a downstream dam

f_s seepage stress

F_s sliding stress generated by gravity

g gravitational acceleration

h slide thickness

h_r the maximum residual dam height

H_t upstream water level

H_{ti} water level at each of the four measuring points

h_w initial difference of impounded water level between the upstream and downstream dam

i hydraulic gradient

k saturated permeability coefficient of dam material

q_b breach discharge of a dam

q_d peak discharge of a downstream dam

q_{in} inflow rate to the reservoir upstream of a dam

q_s seepage discharge through a dam

q_u peak discharge of an upstream dam

R_s resistance stress

s stability coefficient of a downstream dam slope

t_{bo} time from the breach of an upstream dam to overflow of a downstream dam

t_{int} time interval between peak breach discharges of the two dams

α angle of downstream dam slope

θ	slope angle of a residual dam
ρ_d	dry density of a dam material
ρ_w	water density
σ	effective normal stress
φ	internal friction angle of a dam material

References

Awal R, Nakagawa H, Kawaike K, Baba Y, Zhang H (2008) Prediction of Flood/Debris Flow Hydrograph due to Landslide Dam Failure by Overtopping and Sliding. Annuals of Disaster Prevention Research Institute, Kyoto University 51(B), pp. 603–611.

Briaud J (2008), Case Histories in Soil and Rock Erosion: Woodrow Wilson Bridge, Brazos River Meander, Normandy Cliffs, and New Orleans Levees. J. Geotech. Geoenviron. Eng 134(10): 1425-1447.

Cao Z, Yue Z, Pender G (2011) Flood hydraulics due to cascade landslide dam failure. J. Flood Risk Manag 4(2): 104–114.

Chang DS, Zhang LM (2010) Simulation of the erosion process of landslide dams due to overtopping considering variations in soil erodibility along depth. Nat. Hazards Earth Syst. Sci 10(4): 933–946.

Chang, DS, Zhang LM, Xu Y, Huang RQ (2011) Field testing of erodibility of two landslide dams triggered by the 12 May Wenchuan earthquake. Landslides 8: 321–332.

Chen CY, Chang JM (2016) Landslide dam formation susceptibility analysis based on geomorphic features. Landslides 13(5): 1019–1033.

Chen S, Chen Z, Tao R, Yu S, Xu W, Zhou X, Zhou Z (2018) Emergency response and back analysis of the failures of earthquake triggered cascade landslide dams on the Mianyuan River, China. Nat. Hazards Rev 19(3): 05018005.

Chen SC, Lin TW, Chen CY (2015) Modeling of natural dam failure modes and downstream riverbed morphological changes with different dam materials in a flume test. Eng Geol 188: 148–158.

Clague J, and Evans G (1994) Formation and failure of natural dams in the Canadian Cordillera. Geological Survey of Canada Bulletin 464.

Coleman SE, Andrews DP, Webby MG (2002) Overtopping breaching of noncohesive homogeneous embankments. J Hydraul Eng 128(9): 829–838.

Costa JE, and Schuster RL (1988) The formation and failure of natural dams. Geol. Soc. Am. Bull 100(7): 1054–1068.

Cui P, Zhou GGD, Zhu XH, Zhang JQ (2013) Scale amplification of natural debris flows caused by cascading landslide dam failures. Geomorphology 182: 173–189.

Davies T, Manville V, Kunz M, Donadini L (2007) Modeling landslide dambreak flood magnitudes: Case study. J. Hydraul. Eng.,133 (7): 713–720.

Dong JJ, Li YS, Kuo CY, Sung RT, Li MH, Lee CT, Chen CC, Lee WR (2011) The formation and breach of a short-lived landslide dam at Hsiaolin village, Taiwan-part I: Post-event reconstruction of dam geometry. Eng Geol 123(1): 40–59.

Fan X, Westen CJV, Xu Q, Gorum T, Dai FC (2012) Analysis of landslide dams induced by the 2008 Wenchuan earthquake. J Asian Earth Sci 57(6): 25–37.

Gong WP, Juang CH, Wasowski J (2021) Geohazards and human settlements: Lessons learned from multiple relocation events in Badong, China–Engineering geologist's perspective. Eng Geol 285: 106051.

Gregoretti C, Maltauro A, Lanzoni S (2010) Laboratory Experiments on the Failure of Coarse Homogeneous Sediment Natural Dams on a Sloping Bed. J Hydraul Eng 136(11): 868–879.

Fritz HM, Hager WH, Minor HE (2004) Near field characteristics of landslide generated impulse waves. J. Waterw. Port Coast. Ocean Eng 130 (6): 287–302.

Hancox GT, Mc T, Saveney MJ, Manville V, Davies T (2005) The October 1999 Mt Adams rock avalanche and subsequent landslide dam-break floods and effects in Pourea River, Westland, New Zealand. N.Z. J. Geol. Geophys 48: 683–705.

Huang R, Fan X (2013) The landslide story. Nat. Geosci 6(5): 325.

Iverson RM, Logan M, LaHusen RG, Berti M (2010) The perfect debris flow? Aggregated results from 28 large-scale experiments. J. Geophys. Res 115: F03005.

Jiang X, Huang J, Wei Y, Niu Z, Chen F, Zou Z, Zhu Z (2018) The influence of materials on the breaching process of natural dams. Landslides 15(2): 243–255.

Korup O (2004) Geomorphometric characteristics of New Zealand landslide dams. Eng. Geol. 73, 13–35.

Korup, O (2005) Geomorphic imprint of landslides on alpine river systems, southwest New Zealand. Earth Surf. Process. Landf 30(7): 783–800.

Liao HW, Lee CT (2000) Landslides triggered by the Chi-Chi earthquake. Proceedings of the 21st Asian conference on remote sensing, 383–388.

Niu Z, Xu W, Li N, Xue Y (2012) Experimental investigation of the failure of cascade landslide dams. J. Hydrody. 24(3): 430–441.

Peng M, Jiang Q, Zhang Q, Hong Y, Jiang M, Shi Z, Zhang L (2019). Stability analysis of landslide dams under surge action based on large-scale flume experiments. Eng Geol 259:105191.

Peng M, Ma CY, Chen HX, Zhang P, Zhang LM, Jiang MZ, Zhang QZ, Shi ZM (2021). Experimental study on breaching mechanisms of landslide dams composed of different materials under surge waves. Eng Geol 291: 106242.

Peng M, Zhang LM (2012) Breaching parameters of landslide dams. Landslides 9(1): 13–31.

Peng M, Zhang LM, Chang DS, Shi ZM (2014) Engineering risk mitigation measures for the landslide dams induced by the 2008 Wenchuan earthquake. Eng Geol 180: 68–84.

Powledge GR, Ralston DC, Miller P, Chen YH, Clopper PE, Temple DM (1989) Mechanics of overflow erosion on embankments. II: hydraulic and design considerations. J Hydraul Eng 115 (8): 1056–1075.

Risley JC, Walder JS, Denlinger RP (2006) Usoi Dam wave overtopping and flood routing in the Bartang and Panj Rivers, Tajikistan. Nat. Hazards 38(3): 375–390.

Schmocker L, Hager WH (2009) Modelling dike breaching due to overtopping. J Hydraul Res 47(5): 585–597.

Semenza E, Ghirotti M (2000) History of the 1963 Vaiont slide: the importance of geological factors. Bull. Eng. Geol. Environ. 59(2), 87–97.

Shan Y, Chen S, Zhong Q (2020) Rapid prediction of landslide dam stability using the logistic regression method. Landslides 17: 2931–2956.

Shen DY, Shi ZM, Peng M, Zhang LM, Jiang MZ (2020) Longevity analysis of landslide dams. Landslides, 17(8): 1797–1821.

Shi ZM, Guan SG, Peng M, Zhang LM, Zhu Y, Cai QP (2015) Cascading breaching of the Tangjiashan landslide dam and two smaller downstream landslide dams. Eng Geol 193: 445–458.

Shi Z, Zheng H, Yu S, Peng M, Jiang T (2018) Application of CFD-DEM to investigate seepage characteristics of landslide dam materials. Comput. Geotech. 101: 23–33.

Strom A (2010) Landslide dams in Central Asia region. Journal of the Japan Landslide Society 47(6): 309–324.

Takahashi, T (2007) Debris flows: Mechanics, prediction and countermeasures, Taylor and Francis, London/Balkema, Leiden, The Netherlands.

Walder JS, Iverson RM, Godt JW, Logan M, Solovitz SA (2015) Controls on the breach geometry and flood hydrograph during overtopping of noncohesive earthen dams. Water Resour. Res 51(8): 6701–6724.

Wang HB, Sassa K, Xu WY (2007) Analysis of a spatial distribution of landslides triggered by the 2004 Chuetsu earthquakes of Niigata Prefecture, Japan. *Nat. Hazards* 41(1): 43.

Wang Z, Melching CS, Duan X, Yu G (2009) Ecological and hydraulic studies of step-pool systems. J Hydraul Eng 135(9): 705–717.

Wang Z, Cui P, Yu G, Zhang K (2012) Stability of landslide dams and development of knickpoints. Environ Earth Sci 65(4): 1067–1080.

Xu FG, Yang XG, and Zhou JW (2015) Experimental study of the impact factors of natural dam failure introduced by a landslide surge. Environ Earth Sci 74(5): 4075–4087.

Zhao H, Zhang L, Xu Y (2013) Variability of geotechnical properties of a fresh landslide soil deposit. Eng Geol 166(8): 1–10.

Zheng H, Shi Z, Peng M, Yu S (2018) Coupled CFD-DEM model for the direct numerical simulation of sediment bed erosion by viscous shear flow. Eng Geol 245: 309–321.

Zheng H, Shi Z, Shen D, Peng M, Hanley KJ, Ma C, Zhang L (2021) Recent advances in stability and failure mechanisms of landslide dams. Front. Earth Sci 9:659935.

Zhou GGD, Cui P, Chen HY, Zhu XH, Tang JB, Sun QC (2013) Experimental study on cascading landslide dam failures by upstream flows. Landslides 10(5): 633–643.

Zhou GGD, Zhou M, Shrestha MS, Song D, Choi CE, Cui K, Peng M, Shi Z, Zhu X, Chen H (2019) Experimental investigation on the longitudinal evolution of landslide dam breaching and outburst floods. Geomorphology 334: 29–43.

Supplementary Information for "Amplification effect of cascading breach discharge of landslide dams"

Hongchao Zheng[1], Zhenming Shi[1], Ming Peng[1]*, Shenggong Guan[2]*, Kevin J Hanley[3], Shijin Feng[1]

[1]Key Laboratory of Geotechnical and Underground Engineering of the Ministry of Education, and Department of Geotechnical Engineering, College of Civil Engineering, Tongji University, China

[2]Key Laboratory of Rock Mechanics and Geohazards of Zhejiang Province, Shaoxing University, China

[3]School of Engineering, Institute for Infrastructure and Environment, The University of Edinburgh, United Kingdom

*corresponding author: Ming Peng, E–mail: pengming@tongji.edu.cn

Shenggong Guan, E–mail: guanshg@163.com

Contents:

Fig. S1. Experimental dam materials in various components

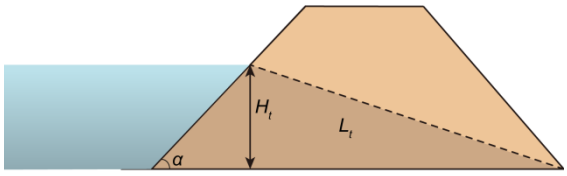

Fig. S2. Calculation of seepage discharge. $q_s = vA = vwH_t/\sin(\alpha)$, where v is the seepage velocity, A is the area, w is the dam length (0.8 m), H_t is the water level and α is the slope of the dam. $v = ki = kH_t/L_t$, where k is the permeability coefficient (Table 1) and L_t is the seepage path.

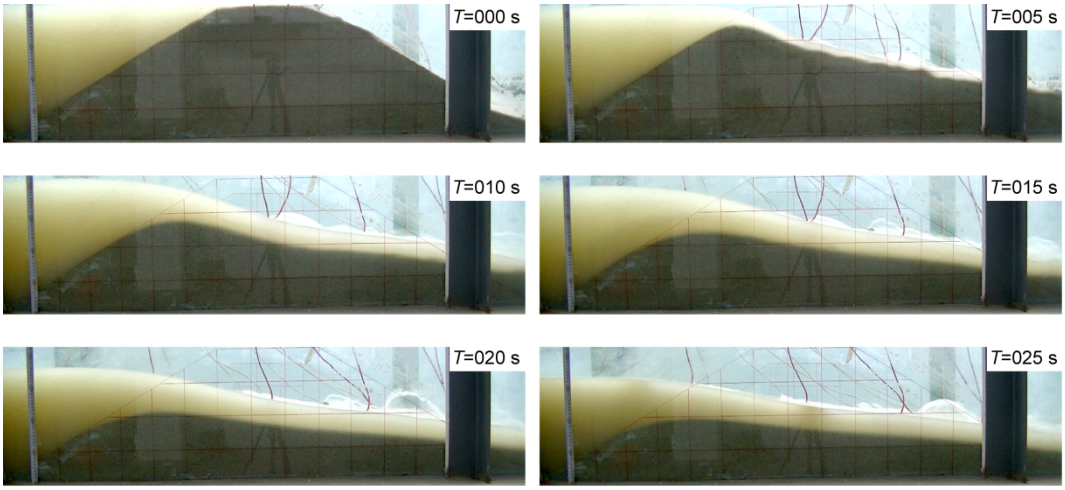

Fig. S3. Cascading breach process of a downstream fine-grained dam from side view (test C1). T is the time elapsed when overtopping flow propagated through the guiding slot. The definition of T is the same for the following Figs. S4 and S5. The water depth was smaller than the dam height at $T = 0$ because overflow migrated in the guiding slot with depth 5 cm.

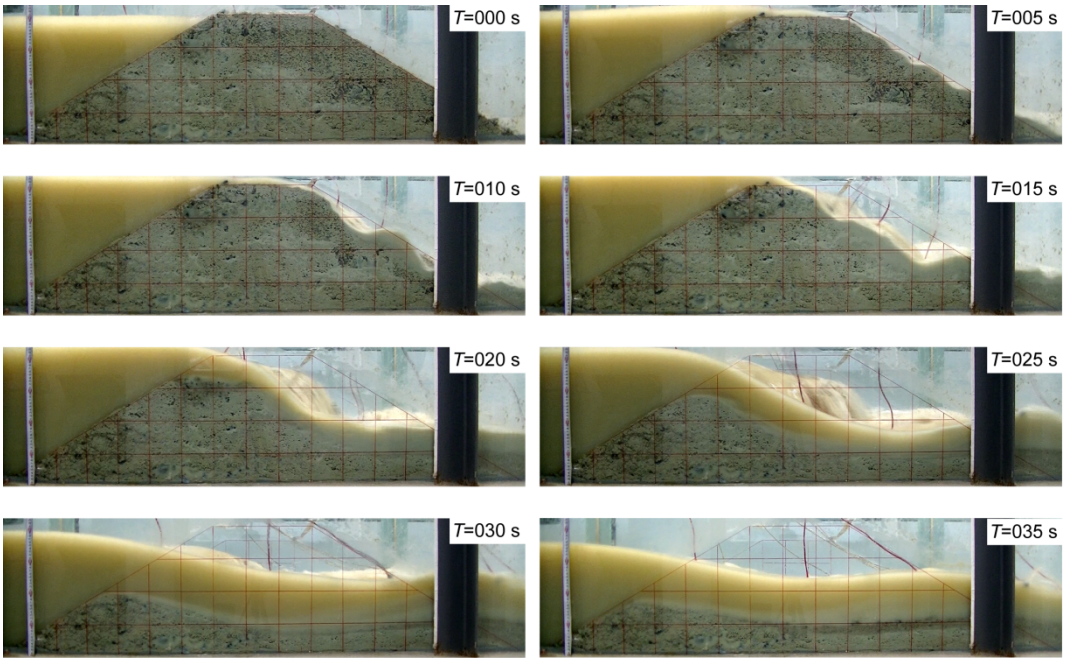

Fig. S4. Cascading breach process of a downstream well graded dam from side view (test C2).

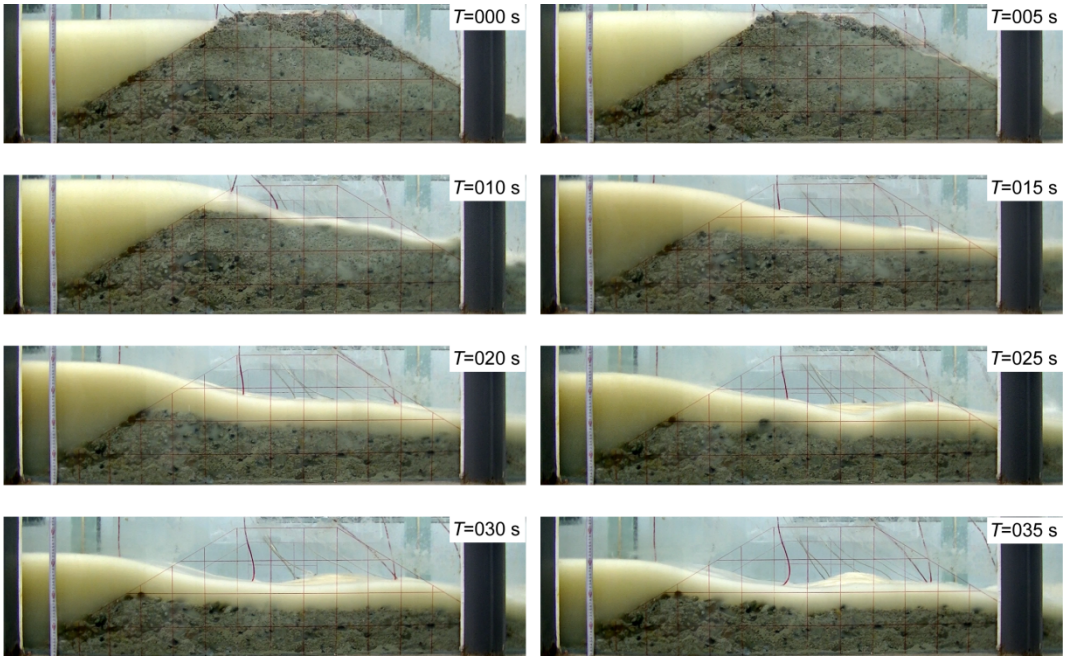

Fig. S5 Cascading breach process of a downstream coarse-grained dam from side view (test C3).

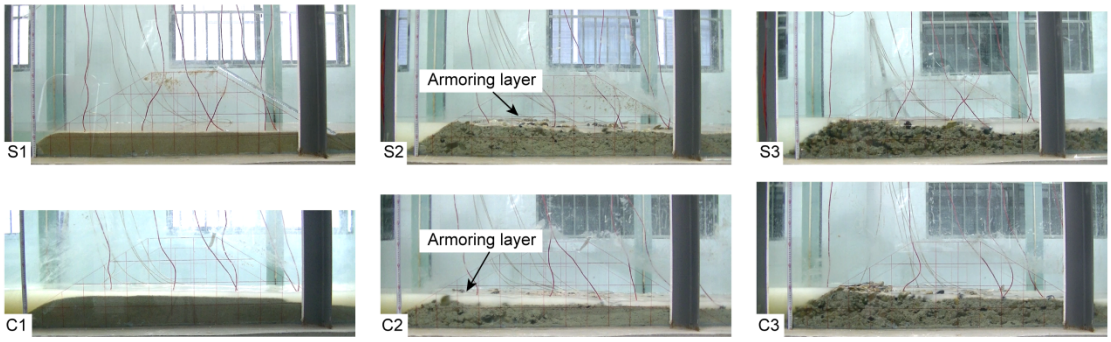

Fig. S6. Residual dams in tests S1–S3 and C1–C3 from side view. An armoring layer was formed on the surfaces of well graded landslide dams.

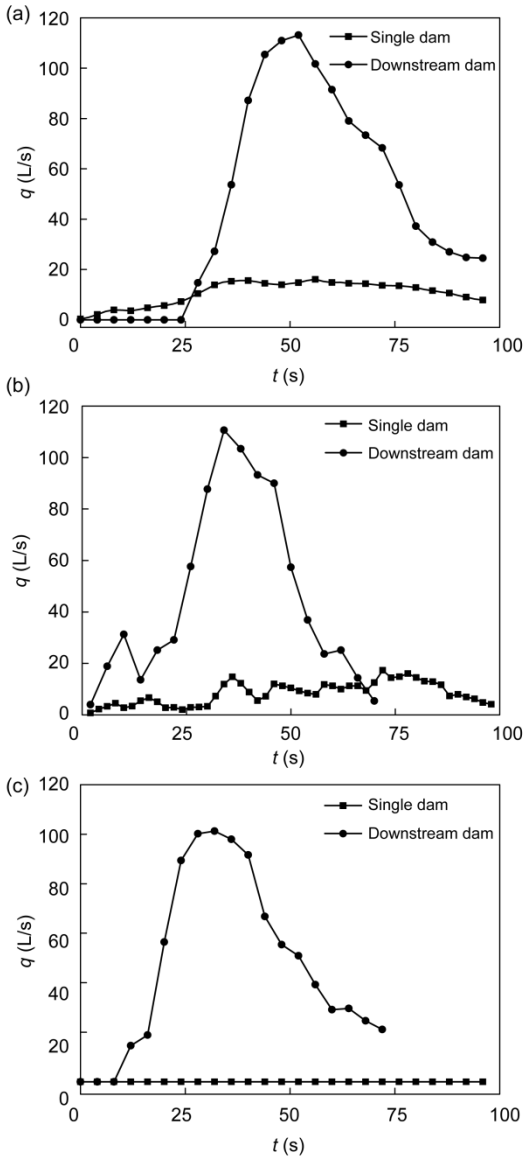

Fig. S7. Comparisons of the breach discharges between the single dams and downstream dams in the cascading tests. (a), (b) and (c), Comparisons of fine-grained, well graded and coarse-grained dams. The single landslide dam with coarse-grained debris did not fail at the inflow rate of 1.13 L/s and the peak breach discharge was equal to the inflow rate.

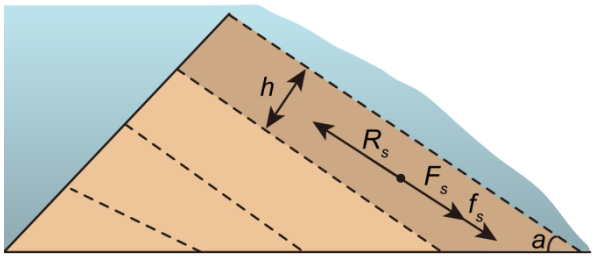

Fig. S8. Stability analysis of seepage stress on a dam downstream. h is the slide depth, α is the slope angle, F_s is the sliding stress generated by gravity, R_s is the resistance stress and f_s is the seepage stress. The seepage stress is assumed to act in the direction of the downstream slope. The shear stress exerted by the breach flood is not considered for a simplified calculation.